nature geoscience

ARTICLES

PUBLISHED ONLINE: 4 SEPTEMBER 2017 | DOI: 10.1038/NGEO3018

Comprehensive characterization of atmospheric organic carbon at a forested site

James F. Hunter[1,2], Douglas A. Day[3,4], Brett B. Palm[3,4], Reddy L. N. Yatavelli[3,4,5], Arthur W. H. Chan[6,7], Lisa Kaser[8,9], Luca Cappellin[10,11], Patrick L. Hayes[3,4,12], Eben S. Cross[2,13], Anthony J. Carrasquillo[1], Pedro Campuzano-Jost[3,4], Harald Stark[3,4,13], Yunliang Zhao[6,14], Thorsten Hohaus[13,15], James N. Smith[9,16], Armin Hansel[8], Thomas Karl[17], Allen H. Goldstein[6], Alex Guenther[9,18], Douglas R. Worsnop[13,19,20], Joel A. Thornton[21], Colette L. Heald[1,22], Jose L. Jimenez[3,4] and Jesse H. Kroll[1,23]*

Atmospheric organic compounds are central to key chemical processes that influence air quality, ecological health, and climate. However, longstanding difficulties in predicting important quantities such as organic aerosol formation and oxidant lifetimes indicate that our understanding of atmospheric organic chemistry is fundamentally incomplete, probably due in part to the presence of organic species that are unmeasured using standard analytical techniques. Here we present measurements of a wide range of atmospheric organic compounds—including previously unmeasured species—taken concurrently at a single site (a ponderosa pine forest during summertime) by five state-of-the-art mass spectrometric instruments. The combined data set provides a comprehensive characterization of atmospheric organic carbon, covering a wide range in chemical properties (volatility, oxidation state, and molecular size), and exhibiting no obvious measurement gaps. This enables the first construction of a measurement-based local organic budget, highlighting the high emission, deposition, and oxidation fluxes in this environment. Moreover, previously unmeasured species, including semivolatile and intermediate-volatility organic species (S/IVOCs), account for one-third of the total organic carbon, and (within error) provide closure on both OH reactivity and potential secondary organic aerosol formation.

Reactive organic species (carbon-containing compounds other than methane, CO, and CO_2) play a central role in the chemistry of the atmosphere in numerous respects: they can directly impact human and ecosystem health, they influence atmospheric oxidant levels, and their oxidation products include secondary species such as ozone and secondary organic aerosol (SOA). However, our ability to model such processes is limited by our incomplete understanding of the amount, identity, and chemistry of atmospheric organic compounds. Ambient (field) measurements have revealed a number of large gaps in our understanding of key atmospheric chemical quantities, including secondary organic aerosol[1], total OH reactivity[2], and total non-methane organic carbon[3]. Such gaps strongly suggest that a substantial fraction of atmospheric organic carbon remains essentially unmeasured and uncharacterized. This places severe limits on our ability to describe the overall lifecycle (emission, reactivity, and loss) and impacts of atmospheric organic compounds. The detection, characterization, and quantification of this unmeasured carbon is thus central for the accurate modelling of air quality, ecological health, and global climate.

However, such measurements face significant analytical challenges. A very large number of organic species are emitted into the atmosphere, and exhibit extraordinary diversity in terms of chemical structure, properties, and reactivity[4]. All are subject to atmospheric oxidation, leading to the formation of new oxidized organic products, exponentially increasing the number and diversity of atmospheric organic species[5]. Volatilities of atmospheric organic compounds span an exceedingly wide range, from volatile organic

[1]Department of Civil and Environmental Engineering, Massachusetts Institute of Technology, Cambridge, Massachusetts 02139, USA. [2]Department of Materials Science and Engineering, Massachusetts Institute of Technology, Cambridge, Massachusetts 02139, USA. [3]Cooperative Institute for Research in Environmental Sciences, University of Colorado, Boulder, Colorado 80309, USA. [4]Department of Chemistry and Biochemistry, University of Colorado, Boulder, Colorado 80309, USA. [5]California Air Resources Board, El Monte, California 91731, USA. [6]Department of Environmental Science, Policy and Management, University of California, Berkeley, California 94720, USA. [7]Department of Chemical Engineering and Applied Chemistry, University of Toronto, Toronto, Ontario M5S 3E5, Canada. [8]Institute for Ion Physics and Applied Physics, University of Innsbruck, Innsbruck 6020, Austria. [9]National Center for Atmospheric Research, Atmospheric Chemistry Observations and Modeling Division, Boulder, Colorado 80309, USA. [10]Research and Innovation Centre, Fondazione Edmund Mach, 38010 S. Michele all'Adige, Italy. [11]School of Engineering and Applied Sciences, Harvard University, Cambridge, Massachusetts 02138, USA. [12]Département de Chimie, Université de Montréal, Montréal, Québec H3C 3J7, Canada. [13]Aerodyne Research Inc., Billerica, Massachusetts 01821, USA. [14]Department of Mechanical Engineering, Carnegie Mellon University, Pittsburgh, Pennsylvania 15213, USA. [15]Department of Energy and Climate Research, IEK-8: Troposphere, Forschungszentrum Juelich, 52425 Juelich, Germany. [16]Department of Chemistry, University of California, Irvine, California 92697, USA. [17]Institute of Atmospheric and Cryospheric Sciences, University of Innsbruck, 6020 Innsbruck, Austria. [18]Department of Earth System Science, University of California, Irvine, California 92697, USA. [19]Department of Physics, University of Helsinki, 00100 Helsinki, Finland. [20]Department of Applied Physics, University of Eastern Finland, 70210 Kuopio, Finland. [21]Department of Atmospheric Sciences, University of Washington, Seattle, Washington 98105, USA. [22]Department of Earth, Atmospheric, and Planetary Science, Massachusetts Institute of Technology, Cambridge, Massachusetts 02139, USA. [23]Department of Chemical Engineering, Massachusetts Institute of Technology, Cambridge, Massachusetts 02139, USA. *e-mail: jhkroll@mit.edu

compounds (VOCs, species present entirely in the gas phase), to intermediate-volatility organic compounds (IVOCs, less-volatile species that are still present only in the gas phase), to semivolatile organic compounds (SVOCs, which can be present in both the gas and condensed phases), to extremely low-volatility organic compounds (ELVOCs, which at equilibrium are found almost entirely in the particle phase)[6–8]. This diversity in properties poses detection and quantification challenges since no one instrument is able to measure or characterize all organic compounds in a given sample. Moreover, S/IVOCs are efficiently lost to inlet/instrument surfaces, and so are not easily measured by standard instrumentation.

Here we describe a first attempt at the comprehensive characterization of atmospheric organic carbon, by integrating measurements taken by multiple state-of-the-art mass spectrometric instruments co-located at a montane ponderosa pine forest site. This work expands on earlier compilations of organic carbon measurements[9–11] by including data from several new analytical instruments that target known gaps in analytical measurements (multifunctional species, S/IVOCs), and examining not only the amount of atmospheric organic carbon but also its key properties (volatility, carbon number, and carbon oxidation state). We present measurements of organic species spanning the entire volatility range found in the atmosphere, from VOCs to low-volatility organic aerosol components, over a range of oxidation states, from reduced to highly oxidized. Such comprehensive measurements allow for closure between top-down and bottom-up measurements of OH reactivity (OHR) and SOA formation, and enable the construction of a measurement-based local budget of atmospheric organic carbon.

Concentrations and properties of organic species

All measurements were made as part of the BEACHON-RoMBAS field campaign, which took place at the Manitou Experimental Forest Observatory in the Colorado Rocky Mountains in July–August 2011[12]. Data were collected by five instruments, three of which were essentially new to field deployment, and included both speciated techniques (measuring individual compounds) and ensemble techniques (characterizing total amounts and average properties of mixtures). The five instruments were: an Aerodyne time-of-flight aerosol mass spectrometer with thermal denuder (TD-AMS)[13,14], measuring ensemble composition and volatility of organic aerosol; a proton transfer reaction time-of-flight mass spectrometer (PTR-MS)[15], measuring speciated VOCs; an acetate-ion chemical ionization time-of-flight mass spectrometer with a micro-orifice volatilization impactor (MOVI-CIMS)[16], measuring speciated gas- and particle-phase organic acids; a semivolatile thermal-desorption aerosol gas chromatograph (SV-TAG)[17], measuring speciated and ensemble elutable (nonpolar) semivolatile species; and a thermal-desorption electron ionization mass spectrometer (TD-EIMS)[18], measuring ensemble composition and volatility of S/IVOCs. All five instruments utilize a high-resolution time-of-flight mass spectrometer (HTOF-MS, Tofwerk AG), providing measurements of elemental formulae of the ions[13], and hence of elemental ratios[19] and carbon oxidation state ($\overline{OS}_C$) (ref. 5). Further, all instruments provide information on either the carbon number (n_C) of the individual species or the effective saturation vapour concentration (c^*) distribution of the ensemble mixture; one can be estimated from the other from expressions relating carbon number, elemental ratios, and volatility[20,21].

Figure 1 shows the combined measurements from all five instruments, each averaged over its entire measurement period. Diurnal profiles and day versus night averages are given in the Supplementary Information; due to the challenges associated with clearly separating various processes (emissions, photochemistry, transport, and so on), here we focus only on campaign averages. Sampling periods for the instruments did not perfectly overlap, but the relative uniformity of the campaign time series indicates that comparisons of campaign averages over different time periods do not introduce major biases (see Supplementary Information). Data are presented within two complementary frameworks for representing complex organic mixtures for visualization and modelling, the $\overline{OS}_C$-versus-c^* space[6] (the 'two-dimensional volatility basis set', or 2DVBS, Fig. 1a), and $\overline{OS}_C$-versus-n_C space[5] (Fig. 1b). Major identified compounds are labelled in Fig. 1b; most remaining markers denote species (or ensembles of species) for which the amount and formula (or average formula) are known, but detailed structures are not.

Figure 1c–e shows the concentration distributions of c^*, n_C, and $\overline{OS}_C$, assuming no overlap between measurements by different instruments (except in unambiguous cases, described in the Supplementary Information). The summed concentration, 26.7 (25.7–28.6) $\mu gC\,m^{-3}$, represents an upper limit to total observed organic carbon. The lower limit, from assuming maximum overlap among the instruments (see Supplementary Information), is not substantially different (22.6 (21.7–24.1) $\mu gC\,m^{-3}$), indicating that overlap in measurements by the different instruments does not have a major effect on the total inferred concentrations.

As shown in Fig. 1, measured organic species span over 19 orders of magnitude in volatility, and exhibit no obvious measurement gaps in any of the dimensions examined. (There are some specific compound classes that may not be measured by this instrument suite; these are likely to be relatively minor, and are discussed in the Supplementary Information.) Each instrument measures organic compounds in a relatively localized region of chemical space, due to the selectivity of each technique (for example, the SV-TAG mostly measures low-$\overline{OS}_C$ species, whereas the CIMS mostly measures higher-$\overline{OS}_C$ species), yet overall the measurements are in general agreement. In areas of measurement overlap (for example, TD-AMS and TD-EIMS), measured values of $\overline{OS}_C$, n_C, and c^* are broadly consistent. This suggests that these five independent instruments provide a self-consistent, and reasonably complete, picture of atmospheric organic carbon.

The measurements in Fig. 1 include relatively little information about the chemical structures of the organic species; obtaining such information would require the use of additional molecular-level (and possibly offline) techniques, but the present online measurements of the amounts and key ensemble properties (c^*, n_C and $\overline{OS}_C$) still reveal broad trends in the measured organic species, and provide insight into the underlying chemistry of the system. In general, concentrations decrease with decreasing volatility (Fig. 1c), increasing carbon number (Fig. 1d), and increasing oxidation state (Fig. 1e). The organic carbon is dominated by relatively volatile, reduced compounds—the primary terpenoid emissions 2-methyl-3-buten-2-ol (MBO) and monoterpenes (the spikes in Fig. 1d at $n_C = 5$ and 10), but also small oxygenates (acetone, methanol, and so on), which can be primary or secondary. Most of the remaining carbon is more oxidized than these species and is likely to be products of oxidation reactions. Reactions of primary emissions can lead to decreases in volatility (via functionalization reactions), to form more oxidized, less-volatile gas-phase species (S/IVOCs) and OA. At the same time, the oxidized species tend to have smaller carbon skeletons (lower n_C) as $\overline{OS}_C$ increases (Fig. 1b), with the vast majority (96%) made up of molecules with 10 or fewer carbon atoms. Only OA is made up predominantly of larger compounds; thus it may be formed from large precursors (for example, sesquiterpenes) and/or oligomerization reactions within the condensed phase. Still, the overall trend of decreasing n_C with increasing $\overline{OS}_C$ suggests the importance of fragmentation reactions during the oxidation of organic species[5]. Such reactions form small, volatile, highly oxidized species, such as formic and oxalic acids (the spikes in Fig. 1e at $\overline{OS}_C = +2$ and $+3$), as well as CO and CO_2 (whose production is difficult to observe). This loss to inorganic carbon, as well as to ongoing deposition[22,23], results in the low levels of organic carbon at high values of $\overline{OS}_C$.

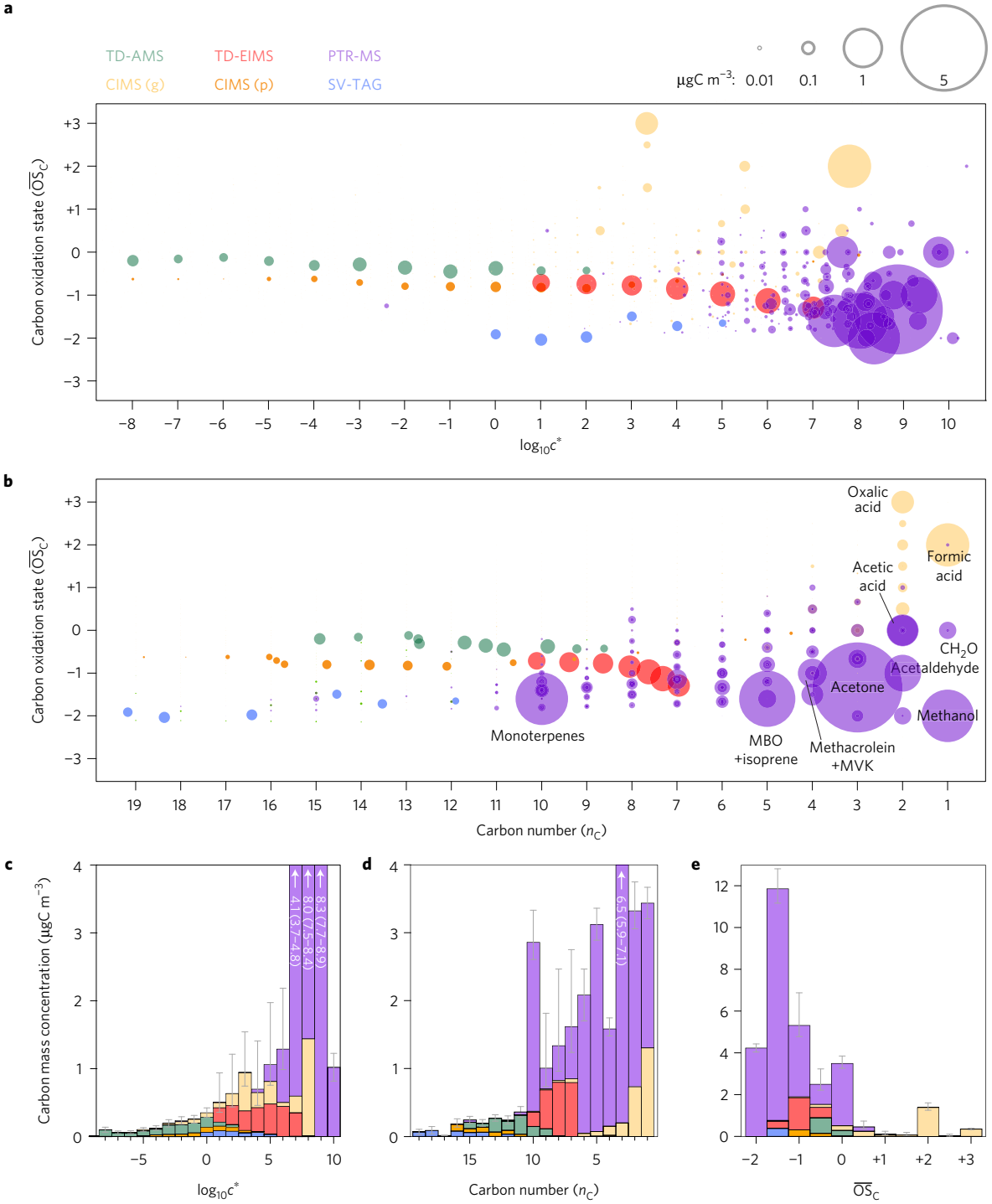

Figure 1 | Campaign-average measurements of non-methane organic carbon loadings and properties during BEACHON-RoMBAS, coloured by analytical technique used (see legend). a,**b**, Plots of carbon oxidation state ($\overline{OS}_C$) versus volatility (c^* at 298 K, μg m^{-3}) and carbon number (n_C), respectively; circle area is proportional to total carbon mass. **c**–**e**, Projections onto the three unique axes in panels **a** and **b**, assuming minimal overlap between the organic species measured by each instrument (see text). Determination of error bars (1σ) is described in the Methods section.

Total observed organic carbon

The measurements presented in Fig. 1 cover a wide and continuous area of chemical space; notably they include S/IVOCs, filling a long-standing measurement gap[24], as well as unspeciated volatile species that are not typically reported. As a result, they cover a substantially larger fraction of the total organic carbon than has been measured in previous field campaigns. Figure 2a shows organic carbon binned into five major classes, defined by their $\overline{OS}_C$, volatility, and atmospheric lifetime: VOCs (reactive, reduced volatile species), OVOCs (reactive, oxidized volatile organic species), long-lived VOCs (LL-VOCs; less-reactive volatile species, with oxidation lifetimes over 1 day), S/IVOCs (gas-phase species with $c^* \leq 10^7$ μg m^{-3}), and OA (particulate organic carbon). OA accounts for only 4% of the measured organic carbon (1.0 μgC m^{-3}). LL-VOCs are the most abundant, accounting for 40% of the measured organic carbon; this may be underestimated somewhat since small (C_2-C_6) alkanes are not measured. VOCs, OVOCs, and S/IVOCs have somewhat lower and approximately equal carbon mass concentrations. The species

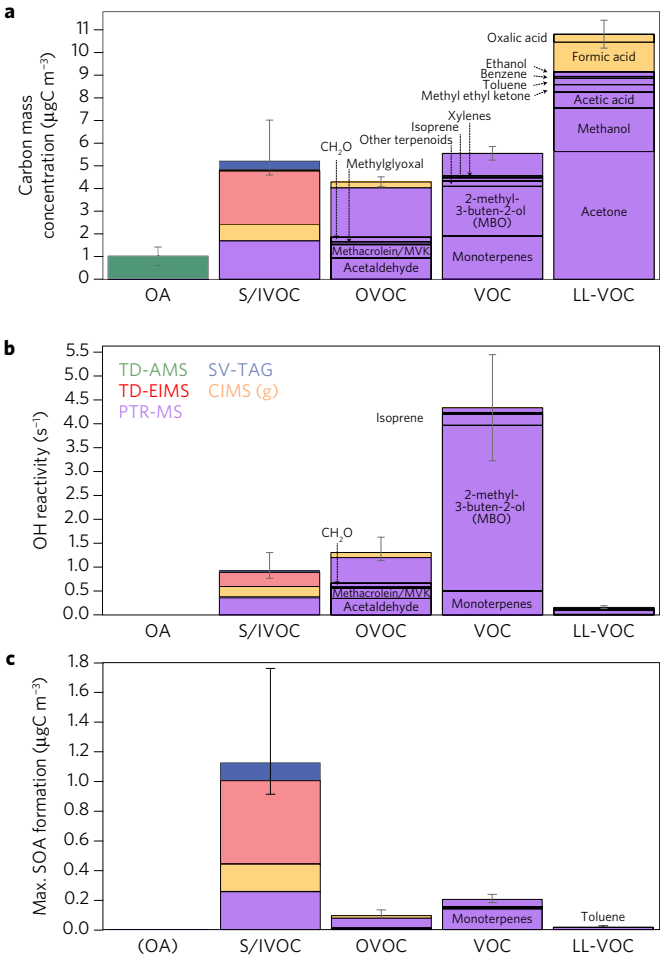

Figure 2 | Total observed organic carbon concentrations, calculated OH reactivity (OHR), and SOA formation, coloured by instrument and organized into major classes of organic species. Gas-phase species are classified into four categories: LL-VOCs ($\tau > 1d$), S/IVOCs ($\tau \leq 1d$, and $c^* \leq 10^7\ \mu g\,m^{-3}$), VOCs ($\tau \leq 1d$, $c^* > 10^7\ \mu g\,m^{-3}$, and $\overline{OS}_C < -1$), and OVOCs ($\tau < 1d$, $c^* > 10^7\ \mu g\,m^{-3}$, and $\overline{OS}_C \geq -1$); error bars, summed for each category, are 1σ. Unlabelled boxes indicate unidentified species or ensemble measurements. It is assumed there is no overlap in measurements by different instruments, so all values represent upper limits. Values of OHR and SOA are calculated as described in the Methods section.

reported for the first time in this study—S/IVOCs and unspeciated (O)VOCs—account for 8.7 (8.1–10.3) $\mu gC\,m^{-3}$ of organic carbon, which represents 31 (29–35)% of the total observed organic carbon (TOOC). Such species were generally not measured/reported in previous field campaigns, and thus measured organic carbon has been traditionally dominated by speciated VOCs and LL-VOCs. For example, in a series of North American field observations, LL-VOCs generally accounted for ≥50% of TOOC, with limited measurements of OVOCs and virtually no measurements of S/IVOCs[9].

While the present measurements of these species enable the characterization of a larger fraction of atmospheric reactive carbon than has previously been possible, the precise extent of carbon closure cannot be assessed fully, given that total organic carbon (TOC) was not measured. While gas-phase TOC instruments have been used in the past[3,25], they were not deployed in the present campaign. At the same time, TOC measurements as single, scalar quantities may be insufficient for fully describing atmospheric organic carbon, since they provide no chemical information, and can overlook key low-volatility species (S/IVOCs, OA) that make up a relatively small fraction of the total.

Closure in OH reactivity and potential SOA formation

Nonetheless, the completeness of the measured suite of organic compounds, and the importance of previously unmeasured species (S/IVOCs and unspeciated (O)VOCs), can be assessed by examining closure for two key atmospheric quantities, OHR and SOA formation. Such closure involves comparison of measurements of the total quantity of interest ('top-down') with the sum of estimated contributions from all individual measured species ('bottom-up'); in most previous studies, for both OHR and SOA formation the bottom-up approach generally underestimates the total, often by a substantial amount[1,2].

OHR is computed from measured concentrations and known/estimated OH rate constants (see Methods). Contributions to OHR from each component (using the upper-limit measurements of organic carbon, Fig. 2a) are given in Fig. 2b. Reactivity is dominated by MBO and reactive terpenoids (isoprene and monoterpenes); these account for 16% of TOOC but 62% of the total OHR, and thus dominate local photochemical activity. The LL-VOCs, a set of small oxygenated VOCs dominated by acetone, methanol, and formic acid, make up only a small fraction (3%) of reactivity despite their large (40%) contribution to TOOC. Unspeciated (O)VOCs and S/IVOCs account for the remaining 25%; this represents a significant, and usually unmeasured, component of OH reactivity. Summed OH reactivity from all measured components is $7 \pm 1\ s^{-1}$ (using the lower-limit concentrations gives a value of $6 \pm 1\ s^{-1}$.) Total (ensemble) OH reactivity was not measured during this campaign, but was found to be $10\ s^{-1}$ at the same site the previous summer[26]. After adjusting for differences in emissions between the two summers (see Supplementary Information), this corresponds to a value of $8 \pm 1\ s^{-1}$ for the present campaign. The agreement between bottom-up and top-down determinations of OH reactivity suggests that the previously unmeasured compounds quantified in this work (S/IVOCs and unspeciated (O)VOCs) are sufficient to account for the missing OH reactivity at this site. In fact, our measurement of a 25% contribution by these species to OHR agrees well with the estimated 30–40% contribution from unmeasured compounds from this site in previous years[26,27].

Top-down measurements of the amount of SOA that can be generated from the OH-initiated oxidation of ambient organic compounds were made using an oxidation flow reactor (OFR), which exposes ambient air to high levels ($3.9–15 \times 10^8$ molecules cm^{-3}) of OH radicals, under conditions in which $RO_2 + HO_2$ reactions dominate[28]. OA formation was always observed; after correction for various loss processes in the reactor (see Supplementary Information), the campaign-average maximum increase in OA carbon was 0.9 (0.6–1.2) $\mu gC\,m^{-3}$. Contributions from individual components, estimated from measured concentrations multiplied by carbon yields (from laboratory studies or estimates, as discussed in Methods) are shown in Fig. 2c. Total SOA formation is calculated to be 1.4 (1.2–2.0) $\mu gC\,m^{-3}$, using the upper-limit measurements, or 0.8 (0.6–1.4) $\mu gC\,m^{-3}$, using the lower-limit measurements; this range is in agreement with the OFR measurements, providing closure (within error) in potential SOA formation. The measured S/IVOCs are critical to this closure, accounting for a large fraction, 78% (74–85%), of the total SOA formation. This highlights the importance of S/IVOCs as SOA precursors; without them, SOA formation from the other measured species is calculated to be only 0.32 (0.29–0.35) $\mu gC\,m^{-3}$, far less than was observed.

Local organic carbon budget

The present measurements, combined with calculated reaction rates and estimates of emission[29] and deposition fluxes[22,30], enable the first construction of an observationally based local budget for

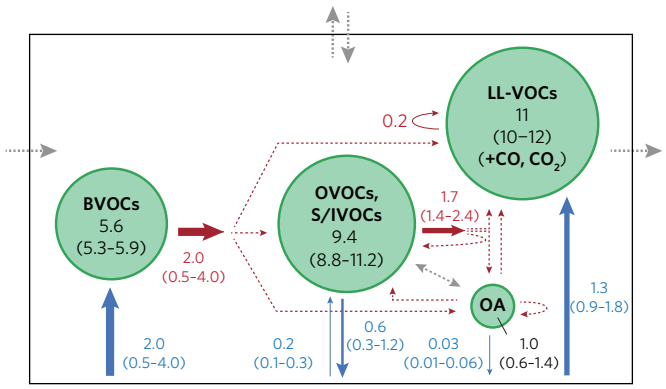

Figure 3 | Observationally constrained budget of atmospheric reactive carbon in the study region, based on campaign-averaged loading measurements and estimated rates of emission, deposition, and oxidation. Units are in μgC m^{-3} (loadings) and μgC m^{-3} h^{-1} (rates); all errors are 1σ. Organic classes are simplified from those in Fig. 2, with VOCs and sesquiterpenes combined into a single BVOC category, and S/IVOCs and OVOCs combined. Arrow colour denotes type of process: red, oxidation; blue, emission/deposition; grey, other physical processes (transport, dilution, partitioning). Dashed arrows denote processes for which rates are largely unconstrained. Calculation details are given in Methods.

atmospheric organic carbon, shown in Fig. 3. Details of these calculations are given in the Methods section.

Reactive biogenic VOCs (BVOCs) dominate the emission of organic carbon (although LL-VOCs are also major contributors). Once emitted, BVOCs oxidize to form a range of products: OVOCs, OA, LL-VOCs, and CO/CO_2. The fate of OVOCs and OA is more complex, since these organic classes may undergo deposition and gas–particle partitioning, as well as oxidation to form other compounds of the same type. (Because of such recycling reactions, denoted by curved arrows, as well as transport, the total flux out does not necessarily equal the total flux in.) Depositional loss of carbon, while uncertain, is dominated by OVOCs and S/IVOCs, consistent with previous work[22,23]. The LL-VOC carbon is largely a 'dead end' with respect to the local oxidation chemistry, since this pool contributes relatively little to the reactivity or SOA formation at the site (Fig. 2). On the timescales accessed in this study (minutes to hours after emission), LL-VOCs are therefore similar to inorganic oxidation products (CO and CO_2). By contrast, most of the remaining species (BVOCs, OVOCs, and S/IVOCs) are associated with large oxidation and deposition rates, indicating that such reactive organic carbon is highly dynamic, with average lifetimes of no more than a few hours.

At the same time, most of these rates are highly uncertain (with typical uncertainties of >50%), or are even completely unconstrained. This highlights our low level of understanding of the processes that govern the atmospheric lifecycle of organic carbon (emission, deposition, and oxidation), and the need for improved constraints on these rates. Centrally important are the product distributions of the oxidation reactions; these include not only the branching among different product classes (for example, the yields of OVOCs, OA, LL-VOCs, and CO/CO_2 from VOC oxidation), but also how molecular species or classes change upon oxidation (that is, their movement through the two-dimensional spaces in Fig. 1), which is poorly constrained at present. Similarly, while the additional organic carbon measured/reported in this work appears to be sufficient, within error, to close longstanding gaps in OH reactivity and SOA formation (Fig. 2b,c), the errors in such estimates remain substantial. These arise predominantly from uncertainties in oxidation rate constants and SOA yields of the unspeciated compounds.

This work thus points to the continuing need for additional process-based (laboratory) studies of the transformation of atmospheric organic carbon from one form to another, using the same types of measurements used in the present field study (ideally in conjunction with more detailed measurements of chemical speciation and structure). These can provide important constraints on the rates, branching, and product distributions of key organic species and classes, particularly those that have not been measured routinely until now. Additionally, this work emphasizes the need for an improved understanding of the coupling of chemistry and dynamics (for example, timescales of chemical reaction versus deposition versus transport) when interpreting field observations and assessing the lifecycle of atmospheric organic carbon.

Methods

Methods, including statements of data availability and any associated accession codes and references, are available in the online version of this paper.

Received 27 April 2017; accepted 1 August 2017; published online 4 September 2017

References

1. Hallquist, M. *et al*. The formation, properties and impact of secondary organic aerosol: current and emerging issues. *Atmos. Chem. Phys.* **9,** 5155–5236 (2009).
2. Yang, Y. *et al*. Towards a quantitative understanding of total OH reactivity: a review. *Atmos. Environ.* **134,** 147–161 (2016).
3. Chung, M. Y., Maris, C., Krischke, U., Meller, R. & Paulson, S. E. An investigation of the relationship between total non-methane organic carbon and the sum of speciated hydrocarbons and carbonyls measured by standard GC/FID: measurements in the Los Angeles air basin. *Atmos. Environ.* **37,** S159–S170 (2003).
4. Goldstein, A. H. & Galbally, I. E. Known and unexplored organic constituents in the Earth's atmosphere. *Environ. Sci. Technol.* **41,** 1514–1521 (2007).
5. Kroll, J. H. *et al*. Carbon oxidation state as a metric for describing the chemistry of atmospheric organic aerosol. *Nat. Chem.* **3,** 133–139 (2011).
6. Donahue, N. M., Kroll, J. H., Pandis, S. N. & Robinson, A. L. A two-dimensional volatility basis set—Part 2: Diagnostics of organic-aerosol evolution. *Atmos. Chem. Phys.* **12,** 615–634 (2012).
7. Donahue, N. M., Robinson, A. L., Stanier, C. O. & Pandis, S. N. Coupled partitioning, dilution, and chemical aging of semivolatile organics. *Environ. Sci. Technol.* **40,** 2635–2643 (2006).
8. Ehn, M. *et al*. A large source of low-volatility secondary organic aerosol. *Nature* **506,** 476–479 (2014).
9. Heald, C. L. *et al*. Total observed organic carbon (TOOC) in the atmosphere: a synthesis of North American observations. *Atmos. Chem. Phys.* **8,** 2007–2025 (2008).
10. de Gouw, J. A. *et al*. Budget of organic carbon in a polluted atmosphere: results from the New England Air Quality Study in 2002. *J. Geophys. Res.* **110,** D16305 (2005).
11. Koss, A. R. *et al*. Photochemical aging of volatile organic compounds associated with oil and natural gas extraction in the Uintah Basin, UT, during a wintertime ozone formation event. *Atmos. Chem. Phys.* **15,** 5727–5741 (2015).
12. Ortega, J. *et al*. Overview of the Manitou Experimental Forest Observatory: site description and selected science results from 2008 to 2013. *Atmos. Chem. Phys.* **14,** 6345–6367 (2014).
13. DeCarlo, P. F. *et al*. Field-deployable, high-resolution, time-of-flight aerosol mass spectrometer. *Anal. Chem.* **78,** 8281–8289 (2006).
14. Huffman, J. A., Ziemann, P. J., Jayne, J. T., Worsnop, D. R. & Jimenez, J. L. Development and characterization of a fast-stepping/scanning thermodenuder for chemically-resolved aerosol volatility measurements. *Aerosol Sci. Technol.* **42,** 395–407 (2008).
15. Graus, M., Müller, M. & Hansel, A. High resolution PTR-TOF: quantification and formula confirmation of VOC in real time. *J. Am. Soc. Mass Spectrom.* **21,** 1037–1044 (2010).
16. Yatavelli, R. L. N. *et al*. A chemical ionization high-resolution time-of-flight mass spectrometer coupled to a Micro Orifice Volatilization Impactor (MOVI-HRToF-CIMS) for analysis of gas and particle-phase organic species. *Aerosol Sci. Technol.* **46,** 1313–1327 (2012).
17. Zhao, Y. *et al*. Development of an *in situ* thermal desorption gas chromatography instrument for quantifying atmospheric semi-volatile organic compounds. *Aerosol Sci. Technol.* **47,** 258–266 (2013).

18. Cross, E. S. *et al*. Online measurements of the emissions of intermediate-volatility and semi-volatile organic compounds from aircraft. *Atmos. Chem. Phys.* **13,** 7845–7858 (2013).
19. Canagaratna, M. R. *et al*. Elemental ratio measurements of organic compounds using aerosol mass spectrometry: characterization, improved calibration, and implications. *Atmos. Chem. Phys.* **15,** 253–272 (2015).
20. Daumit, K. E., Kessler, S. H. & Kroll, J. H. Average chemical properties and potential formation pathways of highly oxidized organic aerosol. *Faraday Discuss.* **165,** 181–202 (2013).
21. Pankow, J. F. & Asher, W. E. SIMPOL.1: a simple group contribution method for predicting vapor pressures and enthalpies of vaporization of multifunctional organic compounds. *Atmos. Chem. Phys.* **8,** 2773–2796 (2008).
22. Nguyen, T. B. *et al*. Rapid deposition of oxidized biogenic compounds to a temperate forest. *Proc. Natl Acad. Sci. USA* **112,** E392–E401 (2015).
23. Park, J.-H. *et al*. Active atmosphere-ecosystem exchange of the vast majority of detected volatile organic compounds. *Science* **341,** 643–647 (2013).
24. Robinson, A. L. *et al*. Rethinking organic aerosols: semivolatile emissions and photochemical aging. *Science* **315,** 1259–1262 (2007).
25. Roberts, J. M., Bertman, S. B., Jobson, T., Niki, H. & Tanner, R. Measurement of total nonmethane organic carbon (C_y): development and application at Chebogue Point, Nova Scotia, during the 1993 North Atlantic Regional Experiment campaign. *J. Geophys. Res.* **103,** 13581 (1998).
26. Kim, S. *et al*. Evaluation of HO_x sources and cycling using measurement-constrained model calculations in a 2-methyl-3-butene-2-ol (MBO) and monoterpene (MT) dominated ecosystem. *Atmos. Chem. Phys.* **13,** 2031–2044 (2013).
27. Nakashima, Y. *et al*. Total OH reactivity measurements in ambient air in a southern Rocky Mountain ponderosa pine forest during BEACHON-SRM08 summer campaign. *Atmos. Environ.* **85,** 1–8 (2014).
28. Palm, B. B. *et al*. *In situ* secondary organic aerosol formation from ambient pine forest air using an oxidation flow reactor. *Atmos. Chem. Phys.* **16,** 2943–2970 (2016).
29. Kaser, L. *et al*. Undisturbed and disturbed above canopy ponderosa pine emissions: PTR-TOF-MS measurements and MEGAN 2.1 model results. *Atmos. Chem. Phys.* **13,** 11935–11947 (2013).
30. Hodzic, A. *et al*. Volatility dependence of Henry's law constants of condensable organics: application to estimate depositional loss of secondary organic aerosols. *Geophys. Res. Lett.* **41,** 4795–4804 (2014).

Acknowledgements

Compilation of the multi-instrument data was supported by NOAA grant NA10OAR4310106. Contributions from individual researchers were supported by NOAA NA10OAR4310106 (J.F.H., E.S.C., A.J.C. and J.H.K.); NSF ATM-0919189, NSF AGS-1243354, and DOE DE-SC0011105 (D.A.D., R.L.N.Y., P.L.H., B.B.P., P.C.-J., H.S. and J.L.J.); US EPA STAR Graduate Fellowship FP-91761701-0 (B.B.P.); NSF RAPID 1135745 (A.W.H.C., Y.Z. and A.H.G.); the Drefyus Foundation (E.S.C.); Austrian Science Fund (FWF) project number L518-N20 (A.H. and L.K.) DOC-FORTE-fellowship of the Austrian Academy of Science (L.K.) and NSF AGS-1238109 (C.L.H.). The SV-TAG, CIMS, and TD-EIMS were developed with support from the DOE SBIR program, grants DE-FG02-08ER85160, DE-FG02-08ER85160, DE-SC0004577, and DE-SC0001666. The authors are grateful to A. Turnipseed and the management of the Manitou Experimental Forest Observatory for field support, to N. Grossberg and B. Lefer for their measurements of boundary layer heights, to N. Kreisberg and S. Hering for their development and support of the SV-TAG, and to A. Steiner for helpful discussions regarding vertical mixing.

Author contributions

Instrument deployment, operation, and data analysis were carried out by: J.F.H., E.S.C., A.J.C. and J.H.K. (TD-EIMS); R.L.N.Y., D.A.D., H.S., J.A.T. and J.L.J. (CIMS); P.L.H., B.B.P., D.A.D., P.C.-J. and J.L.J. (TD-AMS); L.K., L.C., A.H. and T.K. (PTR-MS); A.W.H.C., Y.Z. and A.H.G. (SV-TAG). D.A.D. organized the BEACHON-RoMBAS field campaign along with J.N.S., A.G. and J.L.J. J.F.H. and D.A.D. compiled the multi-instrument data; J.F.H., D.A.D., D.R.W., C.L.H., J.L.J. and J.H.K., interpreted the compiled data set. J.F.H. and J.H.K. wrote the paper. All authors commented on the manuscript.

Additional information

Supplementary information is available in the online version of the paper. Reprints and permissions information is available online at www.nature.com/reprints. Publisher's note: Springer Nature remains neutral with regard to jurisdictional claims in published maps and institutional affiliations. Correspondence and requests for materials should be addressed to J.H.K.

Competing financial interests

E.S.C., H.S., and D.R.W. are employees of Aerodyne Research, Inc. (ARI), which developed and commercialized several of the advanced mass spectrometric instruments utilized in this study.

Methods

Details of the sampling site. Measurements were made at the Manitou Experimental Forest in the Colorado Rocky Mountains, as part of the 'Bio-hydro-atmosphere interactions of Energy, Aerosols, Carbon, H_2O, Organics & Nitrogen—Rocky Mountain Biogenic Aerosol Study' (BEACHON-RoMBAS), running 15 July to 30 August, 2011. The site is located at 2,370 m elevation in the Colorado Rockies, 40 km northwest of Colorado Springs and 70 km southwest of Denver, Colorado (39.10° N, 105.10° W), in a ponderosa pine plantation surrounded by forests with pine, other conifers, and aspen. Details of the site and measurements are described in ref. 12.

Instruments and data analysis. All mass spectrometric measurements used for this analysis were ground-based, with the five instruments located in four temperature-controlled trailers. Sampling height was 25 m for the PTR-MS and 4–5 m for the other instruments.

Thermal Denuder—Aerosol Mass Spectrometer (*TD-AMS*). A high-resolution time-of-flight AMS (Aerodyne Research Inc., Billerica, MA)[13] sampled air downstream of a thermal denuder[14] for 5 min every 30 min from 20 July to 2 Aug and 9 to 30 Aug. The temperature was cycled from ~20 °C to 250 °C and back to ~20 °C every two hours. The AMS quantifies total OA for submicrometre non-refractory particles, and provides calibrated elemental ratios using high-resolution peak fitting, with an empirical correction for biases arising from molecular thermal decomposition and ion fragmentation[19]. For additional details of operation, calibration, and analysis of the HR-ToF-AMS and alternating sampling configuration, see ref. 28. The c^* mass distribution was calculated following the empirical method used in ref. 31. Error in the OC measurement is 40%, based on errors from total organic mass[32] and from elemental ratio determinations[19].

Thermal Desorption–Electron Ionization Mass Spectrometer (*TD-EIMS*). Thermograms of S/IVOC mass spectra were collected every ~11 min using TD-EIMS[18]. The instrument uses cryogenic trapping of the sample followed by temperature-programmed desorption to determine mass concentrations and bulk chemical composition (approximate elemental composition) as a function of volatility, calibrated using *n*-alkanes with known vapour pressures, and reported from $\log(c^*) = 1$ to 7. The TD-EIMS operated for a total of eight days (26 July, 28 to 29 July, and 8 to 12 Aug), collecting 794 individual desorptions. Error in the OC measurement from the TD-EIMS is estimated to be a factor of three in each volatility bin, accounting for variations in collection, desorption, and detection efficiencies for the range of compounds expected in the ambient environment. This reduces to an error of +75%/−25% for the sum of the volatility bins. The instrument precision during α-pinene calibrations is much better (~0.75 μg m^{-3} over the calibration range of 5–15 μg m^{-3}), arising from variability in the collection, desorption and background on a run-to-run basis. Applying this to the ambient average of 3.1 μg m^{-3} gives an error of 28%. Additional details of the calibration procedures and analysis are given in the Supplementary Information.

Micro-orifice volatilization impactor–chemical ionization mass spectrometer (*MOVI-CIMS*). A high-resolution time-of-flight mass spectrometer (Aerodyne Research) using the acetate (CH_3COO^-) reagent ion was used to selectively detect gas and particle-phase organic acids[16]. The MOVI interface allows for both gas-phase analysis during aerosol collection on a stainless steel post and thermal desorption of collected aerosol in ultra-high purity N_2. Data were collected from 20 Aug to 30 Aug at a time resolution of ~1.5 h, yielding a single gas and particle-phase mass spectrum every sampling/analysis cycle. These mass spectra are used for multi-peak fitting yielding identification (elemental formula) and quantifications of 1,374 molecular ions, attributed to acids[33]. Due to the possibility of thermal decomposition of thermolabile species[34,35], particle-phase data are reported as a volatility-resolved ensemble, rather than as individual species. Particle-phase concentrations were calculated using background-subtracted average thermograms of all organic ions (containing C, H, O, and N) identified in the high-resolution mass spectra. Conversion from peak desorption temperature to saturation concentration (c^*) was achieved by measuring calibration thermograms of mixtures of four organic acids[36]. The average thermograms were then fitted to a set of basis functions, whose shapes and positions were determined by the calibration measurements. The areas of these peaks yielded the volatility distributions. To obtain elemental ratios, average thermograms of total signal for O, H, and C were calculated. This results in a larger particle-phase concentration and organic acid fraction of OA (48%) than has been previously reported (29%) for the data set[37], but increases sensitivity to fragment ions resulting from desorption of thermolabile, low-volatility molecules. Measurement error is 5% for known, calibrated compounds. For unknown/uncalibrated compounds, error is estimated to be a factor of three based on the range in calibration slopes of known acids. Applying this error to the individual unknown ions and adding in quadrature gives an ensemble error of 35%. Additional details on instrument configuration, data collection, background subtraction, and data analysis are given elsewhere[37,38].

Proton Transfer Reaction Time-of-Flight Mass Spectrometer (*PTR-MS*). The time-of-flight PTR-MS (IONICON Analytik)[15] collected data from 19 July to 9 Aug. Details of instrument configuration, operation, and calibration are described in ref. 39. High-resolution peak fitting was performed on 30-second averaged raw spectra, fitting 513 peaks in the range m/z 14-391, yielding both signal intensity and elemental formula. Background spectra were fitted separately, spectra were then averaged to 1 h, and then background spectra were subtracted after ion fitting. Ion signals were converted to concentrations using in-field standard calibrations for 10 compound gases and an average sensitivity for the remainder of the peaks. For this analysis, only the 305 compounds containing at least one carbon atom were used. $C_5H_9^+$ ion signal was assigned to MBO (which is primarily measured as $C_5H_{11}O^+$) and isoprene in a 9:1 ratio, based on previous work at the site[29]; $C_3H_7O^+$ was assigned entirely to acetone and $C_2H_5O_2^+$ to acetic acid (rather than propanal and glycolaldehyde, respectively), given the large sources and long lifetimes of those species. For known (calibrated) compounds, error in measured concentrations is 10%. For unknown ions, concentrations were calculated using a relative rate approach with a calibration compound[40]. This contributes an error of 30% per ion, leading to an ensemble error of ~8% when added in quadrature.

Semivolatile Thermal–Desorption Aerosol Gas Chromatograph–Mass Spectrometer (*SV-TAG*). S/IVOCs were measured by the semivolatile thermal–desorption aerosol gas chromatograph/aerosol mass spectrometer (SV-TAG-AMS) from 19 to 30 Aug. The details of the instrument are described in ref. 41. In brief, compounds are collected on a metal fibre filter cell for 90 min, and thermally desorbed in helium carrier gas to a gas chromatograph/mass spectrometer (GC/MS). Authentic standards and deuterated internal standards are used for mass calibration and quantification. A large number of individual species were detected and quantified, but these made up a negligible fraction of TOOC and so here only ensemble measurements (binned by volatility) are reported. Ion signals are separated by their elemental formulae ($C_xH_yO_z^+$) and the hydrocarbon ions ($C_xH_y^+$) quantified using a set of analytical standards[41]. The total ion chromatogram is divided into decadal volatility bins based on the measured retention times and known vapour pressures of *n*-alkanes. Error in measured OC is estimated to be 60%, based on the range of calibration factors found for standards within any individual c^* bin.

Determination of $\overline{OS}_C$, n_C, and c^*. For all instruments, the average carbon oxidation state (of individual species or the ensemble) is determined from the formula $\overline{OS}_C = 2\,O/C - H/C$ (ref. 5). The presence of peroxide and nitrogen-containing groups introduces some errors into this calculation, but unless these moieties are extremely abundant, these errors are small[5]. CIMS and AMS measurements suggest that nitrogen-containing organic species are present in very low abundances (N/C < 0.03) at this site[33,42]. For the ensemble electron ionization instruments (TD-AMS, TD-EIMS, TAG) elemental ratios may be biased by ion fragmentation; however such biases introduce little error to the determination of $\overline{OS}_C$ (ref. 19).

Each instrument also provides measurements of n_C (speciated measurements: CIMS(g), PTR-MS) or c^* (ensemble, thermally separated measurements: TD-AMS, TD-EIMS, CIMS(p), SV-TAG), requiring determination of the remaining quantity. For identified organic species (for example, simple VOCs, OVOCs, and LL-VOCs), literature c^* values[43] are assigned. For other compounds measured by speciated techniques, c^* is estimated from the SIMPOL structure–activity relationship[21], assuming an alkane carbon skeleton and functional groups based on the measured number of oxygen atoms and the best estimate for the functional groups measured. For the CIMS, the first two oxygen atoms are assigned to an acid group and the remaining oxygen atoms to hydroxyl groups, an approach that leads to the strongest agreement between measured and calculated partitioning[38]. For the PTR-MS, oxygen atoms are assigned to carbonyl groups, since molecules with hydroxyl moieties tend to be lost in the unheated inlet of the instrument or to dehydrate upon ionization. In the latter case, this approach may lead to errors in c^* (but not in $\overline{OS}_C$); this effect is difficult to quantify but is unlikely to affect overall results significantly. For the TD-EIMS, TD-AMS, and the SV-TAG, for which c^* distributions are measured, average values of n_C are determined using the approach in ref. 20, assigning a functional group distribution from measured values of c^*, O/C, and H/C. This approach assigns all double bond equivalents to carbonyl groups, so the presence of C=C double bonds or rings would lead to a modest overestimate in n_C; however, the presence of other common functional groups (for example, peroxides or nitrates) is unlikely to introduce substantial errors in this approach[20]. The high temperatures associated with measurements of low-volatility species (OA and S/IVOCs, as measured by the TD-AMS, TD-EIMS, SV-TAG, and MOVI-CIMS) may lead to thermal decomposition of oligomeric (and other thermolabile) species. In these cases the derived c^* and n_C values correspond not to

the exact values of the ambient species, but instead to effective values associated with both physical partitioning and chemical reaction[34,35].

Reactivity calculations. OH reactivity (Fig. 2b) and reaction rates of the organic species (Fig. 3) were estimated based on rates of reactions with OH, O_3, and NO_3 as well as photolysis. For rate calculations, diurnally averaged concentrations of [OH] $= 2.0 \times 10^6$ molec cm^{-3} (ref. 26), [O_3] $= 9.8 \times 10^{11}$ molec cm^{-3} (ref. 12), and [NO_3] $= 4.9 \times 10^6$ molec cm^{-3} (ref. 42) were used. Rate coefficients were taken from the literature when available (see Supplementary Table 1), and a 30% uncertainty is assumed. For unidentified species, oxidation is assumed to be driven by H-atom abstraction by OH, with rate coefficients estimated using the relationship given in ref. 44. This method accounts for differences in the rate coefficient due to the number of carbon, hydrogen, and hydrogen atoms, as well as the 'trapping effect,' wherein oxidation slows for lower-volatility compounds partitioned in the condensed phase. A factor of three uncertainty is used for these estimated OH rate coefficients. If C=C double bonds are an abundant moiety in the unidentified species, oxidation rates (due to reaction with OH, NO_3, or O_3) may be substantially faster. Unfortunately, given the importance of cyclic structures in biogenic species, the abundance of C=C bonds cannot be determined from the present measurements.

SOA formation calculations. The aerosol mass formed after oxidation (Fig. 2c) was calculated from measured SOA carbon yields, assuming this is the maximum SOA formed from a given precursor. Oxidative processes that are likely to be unimportant within the OFR, such as aqueous-phase oxidation, were not considered. For compounds whose SOA yields have been measured in the laboratory at ambient OA loadings and low-NO_x conditions, literature mass yield values were used, and converted to carbon yields using measured OM/OC values (see Supplementary Information). Error is estimated to be 30%. For the remainder of the compounds, carbon yield was parameterized using an approach similar to that in ref. 45, in which yield is a function of the c^* of the precursor. Details of this parameterization are given in the Supplementary Information; uncertainty in these yields is estimated to be a factor of three.

Flux calculations. Emission fluxes of the dominant VOCs, OVOCs and LL-VOCs were taken from flux measurements made at the same site during the previous summer[29,46]. These were taken at nearly the same time of year (3 Aug to 8 Sept, 2010); photosynthetically active radiation (PAR) was slightly higher and temperature was on average 2 °C lower than the present (2011) measurements (see Supplementary Fig. 2). This leads to increased fluxes in 2011 for all species except MBO, which decreased slightly (differences were calculated using the equations given in ref. 29). Flux measurements were of fluxes out of the canopy, meaning that the amount of VOCs that react below the canopy must also be accounted for. This component is estimated by multiplying the measured VOC reaction rate by the average canopy height (16 m), which assumes relatively rapid transport of air out of the canopy. This is added to the out-of-canopy flux to determine the total flux, and then the result divided by the average boundary layer height to determine the column average reaction rate. Although the adjustment for differences in temperature and radiation is fairly robust, it is possible that other differences between 2010 and 2011 (such as rainfall) could lead to differences in the emissions between the two years. Additionally, the measured fluxes are restricted to a relatively small number of compounds with concentrations large enough to be measurable. Because about half of the reactive carbon is made up of unidentified compounds with small concentrations, it is possible that the fluxes could be up to a factor of two larger. This positive error is included in the BVOC flux in Fig. 3.

Oxidation rates were determined using one of two methods, depending on the lifetime of the species. For species whose overall lifetimes are sufficiently long relative to the mixing timescale (1.5 h on average; see Supplementary Information), they are treated as vertically well-mixed, and oxidation rate (μg m^{-3} h^{-1}) is determined by dividing concentration by oxidative lifetime. Shorter-lived species, namely the primary biogenic VOCs (daily average lifetime ~1.2 h) are probably not well-mixed, and thus their ground-level concentrations are unlikely to be representative of the average concentration in the mixed layer. Instead, these short-lived species are assumed to be in steady state, so that their reactive rate can be assumed to be equal to the total emission rate (described above). Uncertainties in oxidation rates (Fig. 3) are calculated from estimated rate coefficients, as described above.

Deposition fluxes were estimated using the approach described in ref. 30. The deposition velocities estimated in this way range from 0 for volatile species and plateau at 4 cm s^{-1} for low-volatility species. These estimated velocities are qualitatively similar to measured deposition velocities reported in ref. 22, where peak velocities in the 1–5 cm s^{-1} range for a variety of organic and inorganic molecules were found. The daily average deposition velocity for formic acid was approximately 0.5 ± 0.2 cm s^{-1}, which is somewhat higher than the calculated value of 0.14 cm s^{-1} used in this study. This difference is probably due to a combination of errors in the calculation methods, and real differences in the two field sites and meteorological conditions. Particle dry deposition velocities were not measured at this site, and so were taken from ref. 47, which gives values of 0.1 to 1.0 cm s^{-1} for vegetated surfaces. An average value of 0.5 cm s^{-1} was used for this analysis. These are somewhat higher than particle deposition velocities measured at other forested sites (0.1 to 0.2 cm s^{-1}) (ref. 48). Uncertainties in deposition velocities are estimated to be a factor of two. Wet deposition is neglected in this budget, but is not expected to dominate given the relatively low precipitation during the measurement period.

Data availability. The data that support the findings of this study are available from the corresponding author upon reasonable request.

References

31. Faulhaber, A. E. *et al*. Characterization of a thermodenuder-particle beam mass spectrometer system for the study of organic aerosol volatility and composition. *Atmos. Meas. Tech.* **2,** 15–31 (2009).
32. Bahreini, R. *et al*. Organic aerosol formation in urban and industrial plumes near Houston and Dallas, Texas. *J. Geophys. Res.* **114,** D00F16 (2009).
33. Stark, H. *et al*. Methods to extract molecular and bulk chemical information from series of complex mass spectra with limited mass resolution. *Int. J. Mass Spectrom.* **389,** 26–38 (2015).
34. Lopez-Hilfiker, F. D. *et al*. Phase partitioning and volatility of secondary organic aerosol components formed from α-pinene ozonolysis and OH oxidation: the importance of accretion products and other low volatility compounds. *Atmos. Chem. Phys.* **15,** 7765–7776 (2015).
35. Isaacman-VanWertz, G. *et al*. Ambient gas-particle partitioning of tracers for biogenic oxidation. *Environ. Sci. Technol.* **50,** 9952–9962 (2016).
36. Stark, H. *et al*. Impact of thermal decomposition on thermal desorption instruments: advantage of thermogram analysis for quantifying volatility distributions of organic species. *Environ. Sci. Technol.* **51,** 8491–8500 (2017).
37. Yatavelli, R. L. N. *et al*. Estimating the contribution of organic acids to northern hemispheric continental organic aerosol. *Geophys. Res. Lett.* **42,** 6084–6090 (2015).
38. Yatavelli, R. L. N. *et al*. Semicontinuous measurements of gas–particle partitioning of organic acids in a ponderosa pine forest using a MOVI-HRToF-CIMS. *Atmos. Chem. Phys.* **14,** 1527–1546 (2014).
39. Kaser, L. *et al*. Comparison of different real time VOC measurement techniques in a ponderosa pine forest. *Atmos. Chem. Phys.* **13,** 2893–2906 (2013).
40. Cappellin, L. *et al*. On quantitative determination of volatile organic compound concentrations using proton transfer reaction time-of-flight mass spectrometry. *Environ. Sci. Technol.* **46,** 2283–2290 (2012).
41. Chan, A. W. H. *et al*. Speciated measurements of semivolatile and intermediate volatility organic compounds (S/IVOCs) in a pine forest during BEACHON-RoMBAS 2011. *Atmos. Chem. Phys.* **16,** 1187–1205 (2016).
42. Fry, J. L. *et al*. Observations of gas- and aerosol-phase organic nitrates at BEACHON-RoMBAS 2011. *Atmos. Chem. Phys.* **13,** 8585–8605 (2013).
43. US EPA *Estimation Programs Interface Suite™ for Microsoft® Windows 8* (2015).
44. Donahue, N. M. *et al*. Why do organic aerosols exist? Understanding aerosol lifetimes using the two-dimensional volatility basis set. *Environ. Chem.* **10,** 151–157 (2013).
45. Donahue, N. M., Robinson, A. L. & Pandis, S. N. Atmospheric organic particulate matter: from smoke to secondary organic aerosol. *Atmos. Environ.* **43,** 94–106 (2009).
46. DiGangi, J. P. *et al*. First direct measurements of formaldehyde flux via eddy covariance: implications for missing in-canopy formaldehyde sources. *Atmos. Chem. Phys.* **11,** 10565–10578 (2011).
47. Zhang, L., Gong, S., Padro, J. & Barrie, L. A size-segregated particle dry deposition scheme for an atmospheric aerosol module. *Atmos. Environ.* **35,** 549–560 (2001).
48. Farmer, D. K. *et al*. Chemically resolved particle fluxes over tropical and temperate forests. *Aerosol Sci. Technol.* **47,** 818–830 (2013).